Nanoscale

Graphene Nanoribbons as Flexible Docks for Chemiresistive Sensing of Gas Phase Explosives

Journal:	*Nanoscale*
Manuscript ID	NR-ART-02-2020-001237.R1
Article Type:	Paper
Date Submitted by the Author:	11-Apr-2020
Complete List of Authors:	Zhang, Jie; University of Texas at Austin Fahrenthold, Eric; University of Texas at Austin, Mech Eng

Graphene Nanoribbons as Flexible Docks for Chemiresistive Sensing of Gas Phase Explosives

Jie Zhang and Eric P. Fahrenthold*

Department of Mechanical Engineering, University of Texas, Austin, TX 78712

E-mail: epfahren@mail.utexas.edu

Abstract

Interpretation of chemiresistive sensor measurements is made difficult by the fact that similar conductance changes may be produced by different adsorbed species. This fundamental ambiguity may be addressed by formulating a new docking paradigm. Instead of decorating graphene with ligands whose structure is well suited to bind with a particular target molecule, a generic dock in the form of a flexible, semiconducting graphene nanoribbon (GNR) may be employed. If the deformed shape of the GNR is then varied, via mechanical actuation, a two dimensional signature (sensor current versus bias voltage and GNR deformation) of the target molecule may be obtained. Ab initio modeling results indicate that this signature may be used to distinguish explosives from background gases and to discriminate between chemically similar explosives.

1 Introduction

Chemiresistive sensing is the focus of much recent research on two dimensional materials.[1,2] In the search for flexible sensors, graphene based devices[3] are of particular interest

since they may combine flexibility with high strength, high electrical conductivity, high thermal stability, and high specific surface area. Experimental and computational research has investigated the use of pristine,[4] functionalized,[5] doped,[6] nanoparticle-decorated,[7,8] and nano-holed[9] graphene for gas phase sensing of various target molecules, including carbon monoxide,[10] nitrogen dioxide,[11] ammonia,[12] and several explosives.[13] Chemresistive sensing offers important advantages in trace detection applications, since signal measurement and electronic packaging methods are well established. However the interpretation of measured conductance changes can be difficult, since similar conductance changes may be produced by different adsorbed species.

Several methods have been suggested which might reduce or eliminate the ambiguities associated with chemiresistive sensor measurements. The first approach is the introduction of sensor arrays. Senesac et al.[14] studied the use of microcantilever arrays designed to distinguish particular analytes, and Meier et al.[15] discuss the statistical analysis of data obtained from such arrays. A second approach is to introduce complimentary sensors, such as nanoresonators[16] or docks,[17] which might be used to measure adsorbed mass or identify adsorbed species. Additional examples include the graphene based mass sensing device of Yang et al.[18] and the sensor system of Muckley et al.[19] which used a quartz crystal microbalance to measure adsorped mass for a carbon nanotube film whose electric resistance was also monitored. A third approach is the development of a single sensor which performs more than one (e.g. chemiresistive and inertial) measurement. Examples are the cantilever based sensor of Boisen et al.,[20] capable of measuring temperature, humidity, and alcohol concentration in water, and the mass spectrometer of Hanay et al.,[21] which used a frequency domain analysis technique to determine in real time both the adsorbate mass and the adsorption position on a nanoresonator. It seems likely that a range of chemical and mechanical transducer mechanisms[22,23] may be needed to perform sensitive and selective trace detection of hazardous gases using flexible, light weight, low power sensors. Hence new sensor designs are of considerable interest.

Employing a series of ab initio calculations, this paper describes a new adaptive sensor for trace detection of explosive molecules. In a nanoelectromechanical system (NEMS), this device might replace an array of conventional chemiresistive sensors, by amending the conventional docking paradigm.[24] Instead of decorating graphene with ligands whose structure is well suited to bind with a particular target molecule, a generic dock in the form of a flexible, semiconducting GNR is first used to adsorb the target molecule. The deformed shape of the GNR is then varied, via mechanical actuation, while the bias voltage is also varied for each deformed shape. Exploiting recent research results[25,26] which describe the current-voltage characteristics of semiconducting nanowires as a function of the voltage bias, the nanowire curvature, and the nanowire length, a two dimensional signature (current versus bias voltage and deformed shape) of the target molecule may be obtained. This chemiresistive signature may then be compared with a computational or experimental data base to identify the analyte. The sections which follow describe the modeling approach, compare the computed signatures of typical background gases and explosive molecules, and highlight the advantages of the adaptive sensor.

2 Computational Model

The chemiresistive sensors modeled in this paper are curved armchair N = 5 graphene nanoribbons (5aGNR) with hydrogen termination, like those shown in Figure 1. The atomic positions are initialized as follows: (a) the center section of length L is composed of four segments, each of length 0.25 L and defined by a radius of curvature R and a rotation θ; the slopes of the center section are zero at its midpoint and at the endpoints; (b) appended to both ends of the center section are mechanical buffers (shown in blue), each of length 0.50 L_{buf}; these buffers are flat and their atomic positions are fixed; (c) appended to the mechanical buffers are electrodes (shown in yellow), each of length 0.50 L_e; these electrodes are flat and their atomic positions are fixed. For all of the calculations shown in this paper,

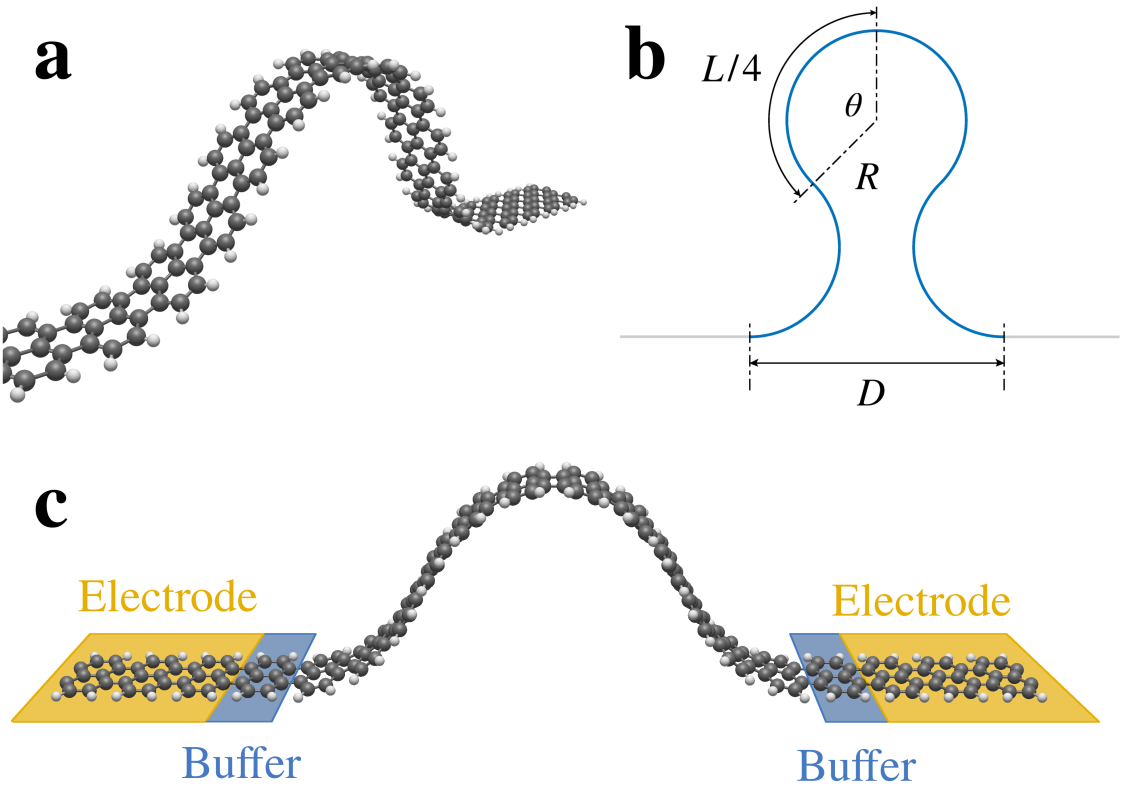

Figure 1: (a) Curved armchair N = 5 graphene nanoribbon, with hydrogen termination. (b) Initial condition configuration for the modeled nanoribbons, defined by a radius of curvature (R), a rotation (θ), and a span (D). (c) The complete computational model included electrodes (shown in yellow) and mechanical buffers (shown in blue), both fixed in place. In the sensor analysis, the atoms in the center section (of length L) were equilibrated in the presence of an analyte molecule.

L_{buf} = 2.0 u.c. and L_e = 6.0 u.c., where 'u.c.' denotes unit cell (for a 5aGNR the unit cell length is 4.28 Å). The initial configurations of the sensors modeled in this paper and the buckled conductors studied in a previous work[26] are in some cases similar. However the equilibrium configurations for the nanoribbons modeled in the two papers will in general be quite different, since adsorption of the target gas molecules will deform both the sensor and the analyte.

As indicated in Figure 1, the separation distance of the mechanical buffers is denoted by D, hereafter referred to as the span. If the span is controlled by a mechanical actuator, for example in a NEMS device, then the computational model defines a family of GNR

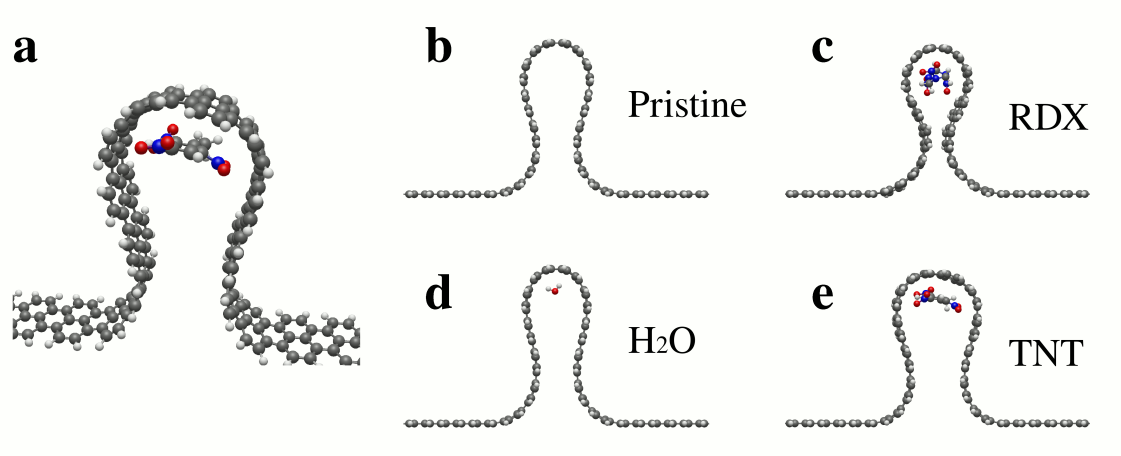

Figure 2: (a) Oblique view of a sensing nanoribbon in equilibrium with an analyte molecule. (b,c,d,e) Equilibrium configurations for a pristine nanoribbon at a bulk strain of -0.69 and corresponding equilibrium configurations for the same nanoribbon interacting with several different analytes. Note that the shape of the deformed nanoribbon sensor varies significantly with the analyte.

sensors described by fabrication lengths L and adjustable spans D. The final set of sensor configurations discussed in this paper takes $L = 51.3$ Å and varies the span over the range:

$$15.9 \text{ Å} \leq D \leq 51.3 \text{ Å} \tag{1}$$

The analysis represents a fixed length sensor with mechanically actuated ends. If mechanical actuation is used to translate the flat electrode/buffer ends along a planar surface, the sensor may be equilibrated in a series of deformed shapes. If the bias voltage is varied in each deformed configuration, current measurements made at each combination of bias voltage and deformed shape produce a two dimensional map of the chemiresistive signature of an adsorbed analyte molecule.

Note that the initialization parameter θ is related to D and L by[25]

$$\frac{D}{L} = \frac{\sin(\theta)}{\theta} \tag{2}$$

Unlike the last cited reference, the initial and the equilibrium configurations of the nanorib-

bons may differ dramatically in shape, for two reasons: (a) the mechanical boundary conditions applied to the nanoribbon sensors modeled here place fewer constraints on the motion, and (2) the nanoribbon sensors modeled here are deformed by their interaction with the adsorbed analytes. At each modeled value of the span, the sensor's chemresistive response was determined by: (a) placing an analyte molecule adjacent to the nanoribbon, on its concave side, and computing the equilibrium configuration of the system, then (b) varying the bias voltage applied to the model electrodes, computing the nanoribbon current at each voltage. Maps of the current versus scaled span (D/L) and bias voltage were produced for six analytes.

The numerical calculations were performed with the ab initio code suite SIESTA,[27] which includes the transport module TranSIESTA,[28] and employs Density Functional Theory and a nonequilibrium Green's function method respectively to determine the equilibrium configurations and the electron transmission. In the equilibrium calculations, the convergence criterion for the maximum atomic force was set to 0.01 eV per angstrom. A local density approximation (LDA)[29] exchange-correlation functional was chosen for the relaxation calculations, and a generalized gradient approximation (GGA) method with the Perdew-Burke-Ernzerhof (PBE)[30] exchange-correlation functional was chosen for the transmission calculations. Double-zeta polarized basis sets were employed for all of the atoms, and the mesh energy cutoff value was set to 300 Ry. Only spin unpolarized cases were modeled.

The current-voltage characteristics of sensors with one adsorbed molecule were computed; the adsorbed molecule was either a background gas (N_2, H_2O, or CO_2) or an explosive molecule (RDX, HMX, or TNT). In each case the bias voltage was varied over the range 0.1 to 0.8 V. The initialization angle (θ) was varied over the range 0 to 134 degrees, which corresponds to a compressive nanoribbon bulk strain (ϵ) range of

$$-0.69 \leq \epsilon \leq 0, \qquad \epsilon = \frac{D}{L} - 1 \tag{3}$$

Figure 2a shows an oblique view of a sensing nanoribbon in equilibrium with an analyte molecule. Figures 2b through 2e compare the equilibrium configuration for a pristine nanoribbon at a bulk strain of -0.69 with corresponding equilibrium configurations for the same nanoribbon interacting with several different analytes. Note that the shape of the deformed nanoribbon sensor varies significantly with the analyte.

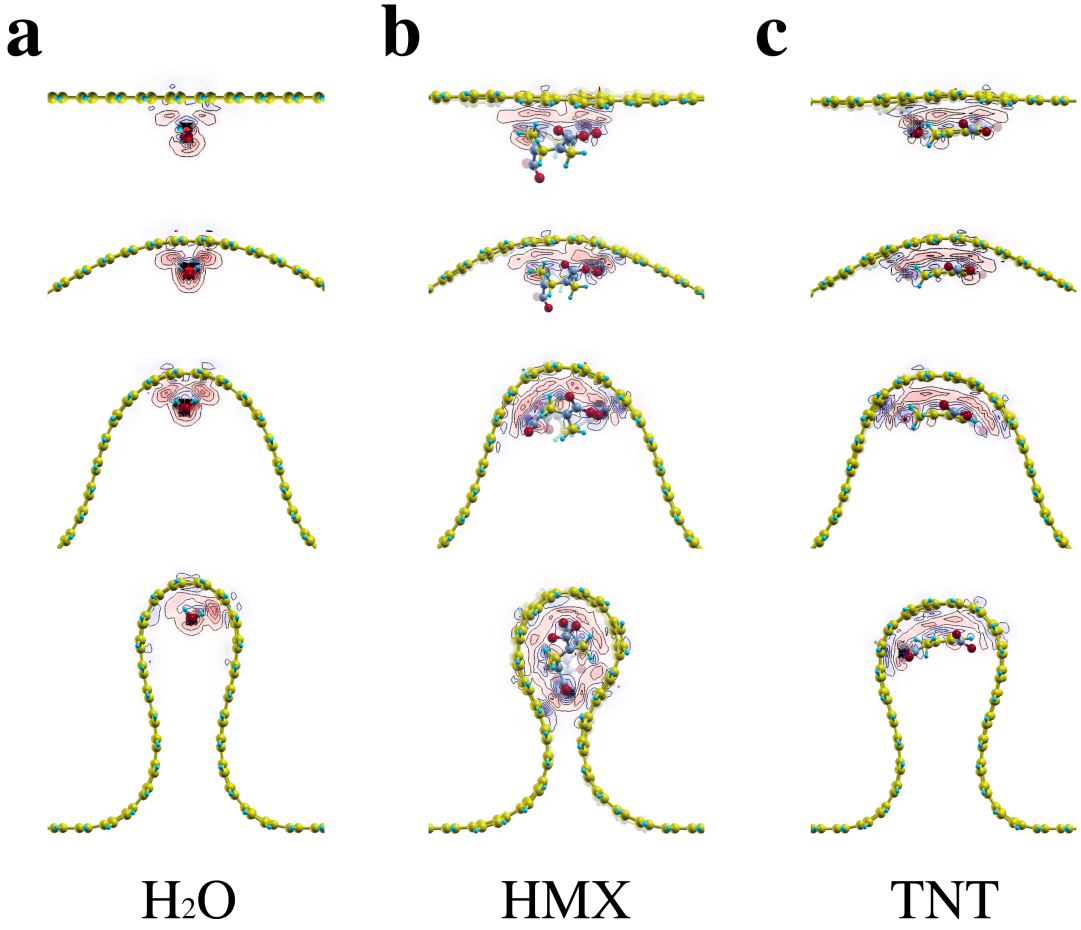

Figure 3: Charge density difference plots for an example background gas molecule and two example explosive molecules; in each series of plots the bias voltage and the nanoribbon length are held constant while the span is varied.

Results and Discussion

Although the chemresistive properties of graphene[31–33] and the variation of semiconducting GNR current with length and curvature[25] have been reported in previous work, the most

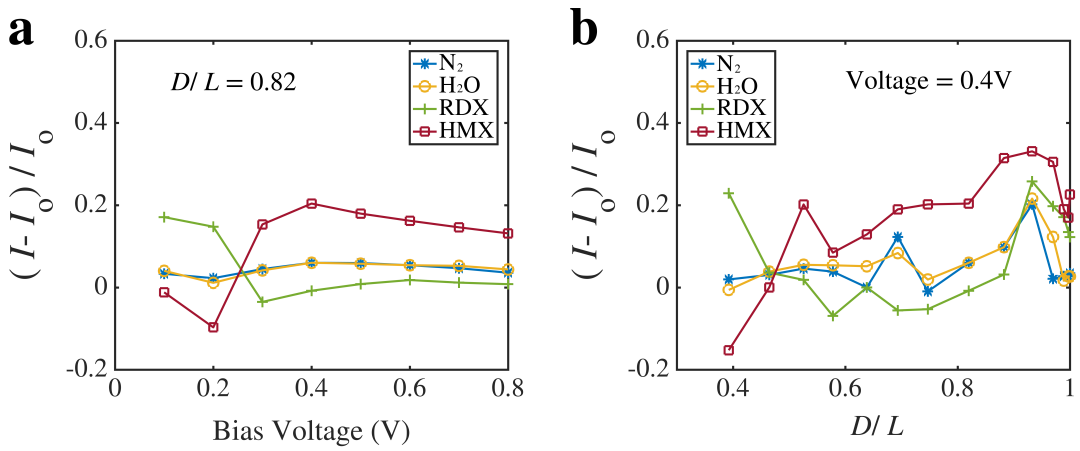

Figure 4: Example plots depicting the variation of the scaled sensor current with bias voltage (V) and scaled span (D/L), for four different analytes. (a) Variation with the applied voltage (at constant bulk strain). (b) Variation with the bulk strain (at constant bias voltage).

important distinguishing feature of the sensor proposed here is the exploitation of these properties in a 'flexible dock' configuration. Figure 3 shows a series of charge density difference plots for an example background gas and two example explosive molecules; in each series of plots the bias voltage and the nanoribbon length are held constant while the span is varied. Both the curvature distribution along the nanoribbon length and the out of plane distortion of the nanoribbon cross section depend upon the span as well as the identity of the sensed molecule, due to differences in the size, structure, and atomic composition of the various analytes. These differences are manifested as changes in the scattering properties (hence the electron transmission) of the sensor-analyte system, whose equilibrium configuration in general involves deformation of both the nanoribbon and the sensed molecule. Computer animations which depict the evolution of the 'docked' (equilibrium) configurations with changes in bulk strain are provided in the Supplementary Materials, for four different analytes.

Since the modeled nanoribbon (5aGNR) is semiconducting, the equilibrium configuration at each separation distance is also associated with a particular current-voltage curve, offering a two-parameter description of the system response which might be employed to identify analytes. Figure 4 shows example plots of the scaled sensor current variations with applied voltage (at constant bulk strain, Figure 4a) and with bulk strain (at constant bias voltage,

Figure 4b) for four different analytes. The scaled current is defined by the ratio $(I - I_o)/I_o$ where I is the sensor current and I_o is the current in the pristine, deformed GNR sensor at the same voltage, in the absence of the analyte. Note that the two background gases show a similar dependance on the bias voltage and the dimensionless span while the two modeled nitramine explosives show marked differences in the scaled sensor current response, despite their chemical similarity.

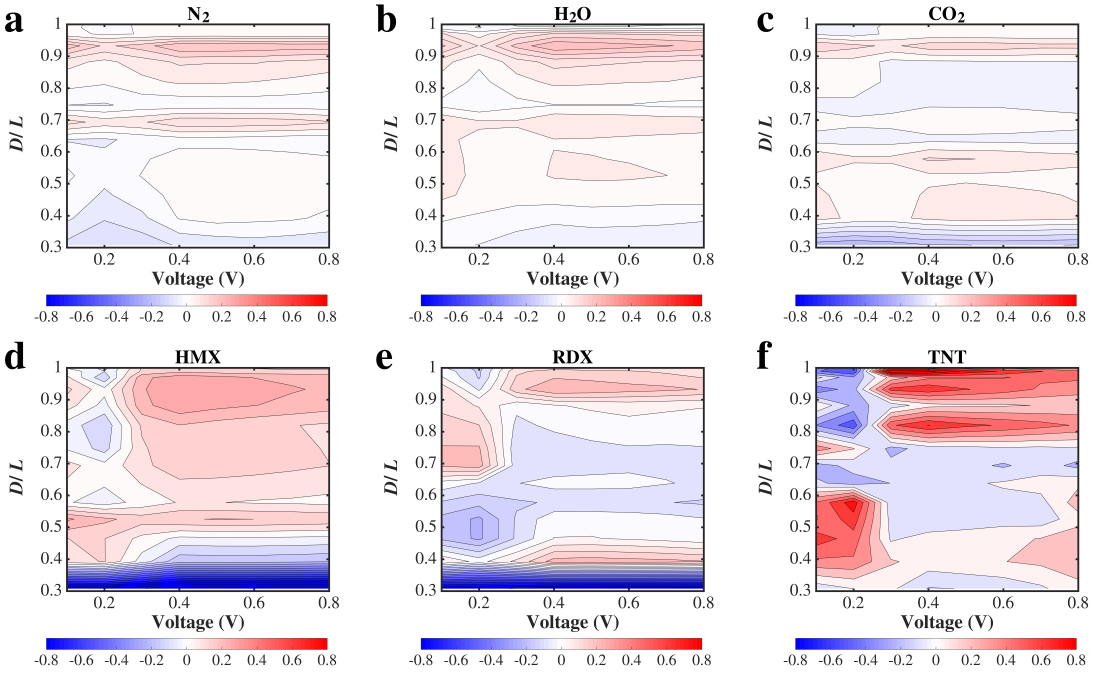

Figure 5: Complete two-parameter response maps for the six modeled analytes (scaled current $(I - I_o)/I_o$ as a function of the scaled span and the bias voltage). The contour plots show positive and negative scaled current changes in red and blue respectively. To facilitate comparison of the sensor responses, all six plots employ the same color bars. (a,b,c) Response of the three modeled background gases. (d,e,f) Response of the three modeled explosives.

The complete two-parameter response maps for the six modeled analytes (scaled current as a function of the scaled span and the bias voltage) are shown in Figure 5. The contour plots show positive and negative scaled current changes in red and blue respectively. To facilitate comparison of the sensor responses, all six plots employ the same color bars. The contour plots for the background gases (Figures 5a, 5b, and 5c) suggest the following conclusions: (a) the sensor responses to the three background gases show a very similar structure; (b) the

magnitudes of the response peaks are modest, as compared to the explosives; and (c) the incremental current depends primarily on the span, with current changes at a constant span a weak function of the bias voltage. The contour plots for the explosives (Figures 5d, 5e, and 5f) suggest the following conclusions: (a) the sensor responses to the three explosives differ markedly from those of the background gases; (b) the incremental currents show a strong dependence on both variables in the two-dimensional parameter space; (c) as compared to the background gases, the positive and negative scaled currents vary over a much larger response range; and (d) the three explosives show marked response differences. The latter differences are most pronounced when comparing TNT to the nitramines, however even the two nitramines show distinct scaled sensor current signatures. Overall the computational results suggest that the proposed sensing scheme can strongly complement explosives detection methods described in the published literature, by adding selectivity to graphene based chemiresistive sensors. The proposed sensing method offers several potential advantages:

- it requires no special fabrication methods beyond those widely studied for graphene nanoribbon production,
- it does not require doping, functionalization, or other chemical treatment of the sensor surface (such treatment is not however precluded),
- it introduces selectivity to widely studied chemresistive sensing methods for graphene devices,
- it employs reversible and controllable mechanical actuation,
- it is amenable to simple vacuum, ultraviolet, or thermal cleaning methods,
- it offers the potential to distinguish chemically similar analytes on the basis of molecule size or structure, and
- it has potential application to a wide range of target molecule types.

Although the sensor concept developed here envisions a NEMS based implementation, application of the proposed sensing scheme could also be accomplished by fabricating[34] a fixed array of curved nanoribbon sensors, of various lengths and for a range of spans, which would accomplish the same selectivity as a single mechanically actuated NEMS device.

The modeling work presented in this paper assumes ideal nanoribbon edges. Realizing that perfectly smooth GNR edges may be difficult to fabricate, and that variations in GNR width can affect conductance,[35] future computational work should investigate the sensitivity of the proposed device to geometric imperfections in the nanoribbons. Since the proposed sensor concept relies on curvature effects in semiconducting nanoribbons, and not on material characteristics unique to graphene, it may well be possible to extend the proposed sensor concept to other two dimensional materials.

Conclusion

This paper describes the first electromechanical extension of widely studied chemiresistive sensing methods for graphene, employing a flexible dock to interact with the analyte. Exploiting recent research results on quantum conductance effects in curved nanoribbons, it suggests the use of NEMS actuation to add selectivity to simple graphene nanoribbon sensors, allowing a single nanoribbon sensor to take the place of a nanoribbon array. Ab initio modling of three background gas molecules and three different explosive molecules indicates that the adaptive sensor can distinguish simple background gases from explosive molecules, as well as distinguish between chemically similar explosives. Recognizing the well known difficulties of trace detection of explosive molecules, the proposed sensing scheme may complement other sensing methods already in use to improve the performance of light weight, low power explosive sensing systems.

Acknowledgments

This work was supported by the Office of Naval Research (Grant number N00014-16- 2357). Computer time support was provided by the Texas Advanced Computing Center at the University of Texas at Austin (Project number G-815029)) and the Department of Defense High Performance Computing Modernization Program (Project number ONRDC40983493).

Supporting Information Available

Animation S1: Comparison of the equilibrium configurations of a fixed length, pristine graphene nanoribbon at various spans with the corresponding configurations in the presence of a background gas or explosive molecule.

Animation S2: Equilibration of a pristine graphene nanoribbon at a fixed span.

Animation S3: Equilibration of a graphene nanoribbon at a fixed span, in the presence of a water molecule.

Animation S4: Equilibration of a graphene nanoribbon at a fixed span, in the presence of an RDX molecule.

Animation S5: Equilibration of a graphene nanoribbon at a fixed span, in the presence of a TNT molecule.

References

(1) Donarelli, M.; Ottaviano, L. 2D Materials for Gas Sensing Applications: A Review on Graphene Oxide, MoS2, WS2 and Phosphorene. *Sensors* **2018**, *18*, 3638.

(2) Meng, Z.; Stolz, R. M.; Mendecki, L.; Mirica, K. A. Electrically-Transduced Chemical

Sensors Based on Two-Dimensional Nanomaterials. *Chemical Reviews* **2019**, *119*, 478–598.

(3) Singh, E.; Meyyappan, M.; Nalwa, H. Flexible Graphene-Based Wearable Gas and Chemical Sensors. *ACS Applied Materials and Interfaces* **2017**, *9*, 34544–34586.

(4) Chen, G.; Paronyan, T. M.; Harutyunyan, A. R. Sub-ppt gas detection with pristine graphene. *Applied Physics Letters* **2012**, *101*, 053119.

(5) Robinson, J. T.; Perkins, F. K.; Snow, E. S.; Wei, Z.; Sheehan, P. E. Reduced graphene oxide molecular sensors. *Nano Letters* **2008**, *8*, 3137–3140.

(6) Liu, L.; Yang, M.; Gao, S.; Zhang, X.; Cheng, X.; Xu, Y.; Zhao, H.; Huo, L.; Major, Z. Co3O4 Hollow Nanosphere-Decorated Graphene Sheets for H2S Sensing near Room Temperature. *ACS Applied Nano Materials* **2019**,

(7) Galstyana, V.; Cominib, E.; Kholmanov, I.; Ponzoni, A.; Sberveglieria, V. Graphene-zinc oxide based nanomaterials for gas sensing devices. *Procedia Engineering* **2016**, *168*, 1172–1175.

(8) Karaduman, I.; Engin, E.; Celikkan, H.; Erk, N.; Acar, S. Room-temperature ammonia gas sensor based on reduced graphene oxide nanocomposites decorated by Ag, Au and Pt nanoparticles. *Journal of Alloys and Compounds* **2017**, *722*, 569–578.

(9) Cagliani, A.; Mackenzie, D.; Tschammer, L.; Pizzocchero, F.; Almdal, K.; Bøggild, P. Large-Area Nanopatterned Graphene For Ultrasensitive Gas Sensing. *Nano Research* **2014**, *7*.

(10) Joshi, R. K.; Gomez, H.; Alvi, F.; Kumar, A. Graphene films and ribbons for sensing of O2, and 100 ppm of CO and NO2 in practical conditions. *The Journal of Physical Chemistry C* **2010**, *114*, 6610–6613.

(11) Novikov, S.; Lebedeva, N.; Satrapinski, A.; Walden, J.; Davydov, V.; Lebedev, A. Graphene based sensor for environmental monitoring of NO2. *Sensors and Actuators B: Chemical* **2016**, *236*, 1054–1060.

(12) Ghosh, R.; Singh, A.; Santra, S.; Ray, S. K.; Chandra, A.; Guha, P. K. Highly sensitive large-area multi-layered graphene-based flexible ammonia sensor. *Sensors and Actuators B: Chemical* **2014**, *205*, 67–73.

(13) Zhang, J.; Fahrenthold, E. P. Graphene-Based Sensing of Gas-Phase Explosives. *ACS Applied Nano Materials* **2019**, *2*, 1445–1456.

(14) Senesac, L.; Thundat, T. G. Nanosensors for trace explosive detection. *Materials Today* **2008**, *11*, 28–36.

(15) Meier, D. C.; Raman, B.; Semancik, S. Detecting chemical hazards with temperature-programmed microsensors: overcoming complex analytical problems with multidimensional databases. *Annual Review of Analytical Chemistry* **2009**, *2*, 463–484.

(16) Parmar, M.; Gangavarapu, P.; Naik, A. Dynamic range tuning of graphene nanoresonators. *Applied Physics Letters* **2015**, *107*, 113108.

(17) Morris, G.; Huey, R.; Lindstrom, W.; Sanner, M.; Belew, R.; Goodsell, D.; Olson, A. AutoDock4 and AutoDockTools4: Automated Docking with Selective Receptor Flexibility. *Journal of Computational Chemistry* **2009**, *30*, 2785–2791.

(18) Yang, Y.-T.; Callegari, C.; Feng, X.; Ekinci, K. L.; Roukes, M. L. Zeptogram-scale nanomechanical mass sensing. *Nano Letters* **2006**, *6*, 583–586.

(19) Muckley, E. S.; Nelson, A. J.; Jacobs, C. B.; Ivanov, I. N. Multimodal probing of oxygen and water interaction with metallic and semiconducting carbon nanotube networks under ultraviolet irradiation. *Journal of Photonics for Energy* **2016**, *6*, 025506.

(20) Boisen, A.; Thaysen, J.; Jensenius, H.; Hansen, O. Environmental sensors based on micromachined cantilevers with integrated read-out. *Ultramicroscopy* **2000**, *82*, 11–16.

(21) Hanay, M. S.; Kelber, S.; Naik, A.; Chi, D.; Hentz, S.; Bullard, E.; Colinet, E.; Duraffourg, L.; Roukes, M. Single-protein nanomechanical mass spectrometry in real time. *Nature Nanotechnology* **2012**, *7*, 602.

(22) Li, Y.; Zhang, Y.; Zare, R. Electrical, Optical, and Docking Properties of Conical Nanopores. *ACS Nano* **2012**, *6*, 993–997.

(23) Mu, B.; Zhang, J.; McNicholas, T.; Reuel, N.; Kruss, S.; Strano, M. Recent Advances in Molecular Recognition Based on Nanoengineered Platforms. *Accounts of Chemical Research* **2014**, *6*, 979–988.

(24) Muthoosamy, K.; Bai, R.; Manickam, S. Graphene and Graphene Oxide as a Docking Station for Modern Drug Delivery System. *Current Drug Delivery* **2014**, *11*, 701–718.

(25) Zhang, J.; Fahrenthold, E. P. Conductance of Curved 3 M–1 Armchair Graphene Nanoribbons. *The Journal of Physical Chemistry C* **2019**, *123*, 21805–21812.

(26) Zhang, J.; Fahrenthold, E. P. Conductance of Buckled N = 5 Armchair Graphene Nanoribbons. *The Journal of Physical Chemistry Letters* **2020**, *11*, 1378–1383.

(27) Soler, J. M.; Artacho, E.; Gale, J. D.; García, A.; Junquera, J.; Ordejón, P.; Sánchez-Portal, D. The Siesta Method for Ab initio Order-N Materials Simulation. *J. Phys-Condens. Mat.* **2002**, *14*, 2745.

(28) Stokbro, K.; Taylor, J.; Brandbyge, M.; Ordejon, P. Transiesta: a Spice for Molecular Electronics. *Ann. N.Y. Acad. Sci.* **2003**, *1006*, 212–226.

(29) Perdew, J. P. JP Perdew, K. Burke, and M. Ernzerhof, Phys. Rev. Lett. 77, 3865 (1996). *Phys. Rev. Lett.* **1996**, *77*, 3865.

(30) Perdew, J. P.; Zunger, A. Self-interaction correction to density-functional approximations for many-electron systems. *Physical Review B* **1981**, *23*, 5048.

(31) Fowler, J. D.; Allen, M. J.; Tung, V. C.; Yang, Y.; Kaner, R. B.; Weiller, B. H. Practical chemical sensors from chemically derived graphene. *ACS Nano* **2009**, *3*, 301–306.

(32) Romero, H. E.; Joshi, P.; Gupta, A. K.; Gutierrez, H. R.; Cole, M. W.; Tadigadapa, S. A.; Eklund, P. C. Adsorption of ammonia on graphene. *Nanotechnology* **2009**, *20*, 245501.

(33) Dan, Y.; Lu, Y.; Kybert, N. J.; Luo, Z.; Johnson, A. C. Intrinsic response of graphene vapor sensors. *Nano Letters* **2009**, *9*, 1472–1475.

(34) Niu, W.; Liu, J.; Mai, Y.; Mullen, K.; Feng, X. Synthetic Engineering of Graphene Nanoribbons with Excellent Liquid-Phase Processibility. *Trends in Chemistry* **2019**, *1*, 549–558.

(35) Takashima, K.; Yamamoto, T. Conductance fluctuation of edge-disordered graphene nanoribbons: Crossover from diffusive transport to Anderson localization. *Applied Physics Letters* **2014**, *104*, 093105.

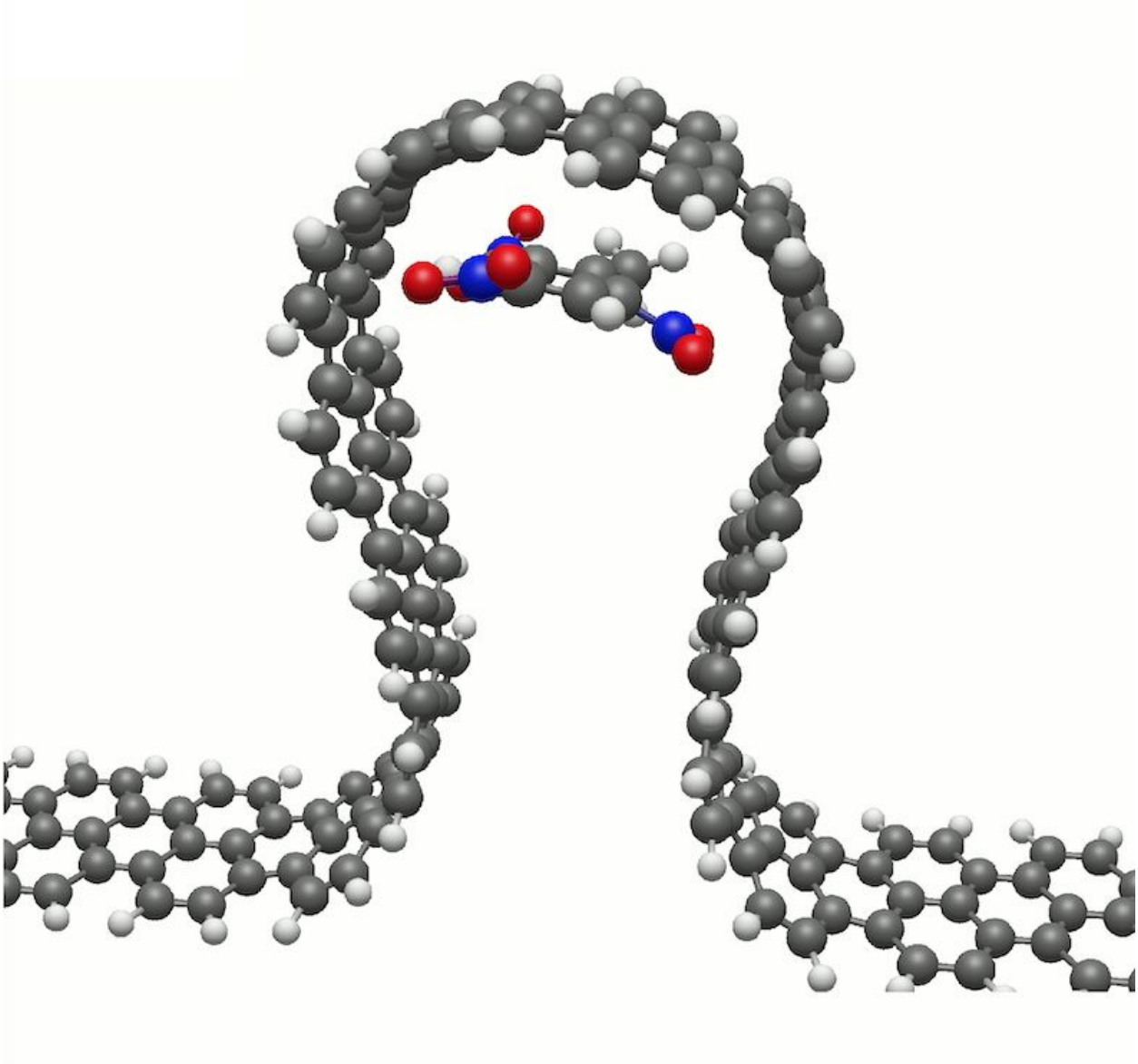

Oblique view of a sensing nanoribbon in equilibrium with an analyte molecule.